CHAPTER 4

*Ag_3PO_4/BiOBr HETEROJUNCTIONS WITH HIGH PHOTOCATALYTIC ACTIVITY AND STABILITY**

4.1. Introduction

BiOBr is an important V-Vi-Vii ternary compound, and belongs to the family of main group multicomponent metal oxyhalides.[1] It is known to exhibit good photocatalytic activity due to the hybridization between O 2p and Bi 6s states.[2,3] It has a layered tetragonal matlockite (PbFCl) structure, and possess unique and excellent electrical, magnetic, optical, and luminescent properties.[4,5] The presence of layered structure helps to polarize the related atoms or orbitals by providing enough large space. The induced dipole can then separate the electron-hole pairs efficiently, and improve the photocatalytic ability.[6]

BiOBr has a unique sandwich like crystal structure consisting of tetragonal $[Bi_2O_2]^{+}$ slices sandwiched between two sheets of Br^- ions, forming a $[Bi_2O_2Br_2]$ layer unit.[7,2] The $[Bi_2O_2Br_2]$ layer units are held by non-bonding (van der waals) interactions through Br atoms along the anisotropic growth direction, which is *c axis*.[7] These nonbonding interactions help the layer units to stock together one by one in an orderly way. There exist strong internal electric field perpendicular to Br^- ions and Bismuth oxide layer in these sandwich like crystals.[8,9] The presence of such strong internal electric fields are believed to enhance the effective separation and conduction of photoinduced electron-hole pairs, which facilitates the redox reaction on the surface of semiconductor, and thereby assist a high photocatalytic activity.[3,8, 9]

Bismuth oxybromide (BiOBr) has been recognised as one of the most promising photocatalysts owing to its lamellar structure,[10] high photocatalytic activity, and photocorrosion stability.[11-16] The good chemical stability and eco-friendly nature makes BiOBr as one of the choicest catalysts for degradation of toxic organic pollutants.[17-21]

To further enhance the photocatalytic activity of BiOBr for practical applications, it is important to decrease the electron-hole recombination to a higher rate. Some research has suggested that the electron-hole recombination in semiconductors can be retarded by constructing molecular electron relay semiconductor structures, or efficient electron transport matrices.[22,23]

**Applied Surface Science 332 (2015) 419-429*

Some researchers have also reported that photocatalytic activity is related to the configuration of the photocatalysts, and therefore tuning of shape and structure could improve the photocatalytic ability of the photocatalyst.[24,25] Moreover, it is notable that the band gap of BiOBr has been reported around (2.9 eV) which limits its absorption above 430 nm.[26] Several strategies, such as impurity doping,[27] surface decoration,[28,29] (metal deposition or heterojunction), photosensitization,[29] and morphology controlled synthesis [30-34] have been employed to broaden the visible light absorption range of such photocatalysts. Though doping has proved to be effective in shifting the absorption edge into the visible range, but the sensitivity of photocatalysts to doping level and homogeneity makes it a less suitable method.[35] Construction of heterostructures by combination of two semiconductors with matching band potentials, such as BiOCl/Bi_2O_3,[36] AgI/BiOI,[37] BiOCl/BiOI,[38] BiOBr/BiOI,[39-41] $Bi_2O_2CO_3$/BiOI,[42] and Bi_2S_3/BiOI[43] has turned out to be more flexible and effective strategy for broadening the visible light absorption of photocatalysts because heterojunction can effectively tune the electronic properties of composites,[36] and are also less sensitive to component homogeneity. For an effective heterojunction with increased visible light absorption and efficient separation of photoinduced charge carriers, the semiconductors should have the matching band structure, requisite band gap energy, and suitable molar ratio.[29,44-46]

4.2. Review of literature

To date, extensive efforts have been made focussing on the development of various synthetic methods for the synthesis of BiOBr and BiOBr based composites.

Three dimensional (3D) nanostructured materials, such as nanosheets and nanoplates with large surface area, nearly perfect crystallinity, structural anisotropy, and quantum confinement effects have attracted much attention in recent years because it is believed that such structures could favour the decrease of electron-hole recombination and facilitate their transfer to the surface.[47] Tian *et al.*[48] reported mesoporous 3D BiOBr microspheres with excellent visible light activity for the removal of bisphenol A. These mesoporous materials have ordered open pore frameworks and high surface area,[49,2] which not only improves the contact of photocatalyst with organic pollutants, but also provides transport paths and more active sites in photocatalytic reaction. Further, these mesoporous materials can harvest visible light more efficiently due to the multiple scattering within the solid frame work.[49,2] Similarly, Tang's group[50] reported three dimensional (3-D) microspherical BiOBr architectures assembled by nanosheets by employing ethylene glycol (EG) assisted solvothermal route. Various other morphologies

of BiOBr with improved catalytic ability have also been reported. For example, Wang *et al.*[26] used hydrolysis method to synthesize highly efficient photocatalytic BiOBr powder using Bi_2O_3 and hydrobromic acid. Similarly, highly visible light active flower like BiOBr microspheres with excellent visible light activity were reported by Huo *et al.*[30]

Recently, ionic liquids (IL) have received considerable attention conducive to the synthesis of functional materials because IL is a good dispersing agent, solvent, and a template.[51-54] Xia *et al.*[55] reported a facile one pot solvothermal synthesis of highly visible light active Bi_2WO_6/BiOBr in presence of reactive ionic liquid [C16mim] Br. They reported that [C16mim] Br acts as solvent, reactant, and template at the same time.

In the recent past, microwave assisted synthetic routes have been reported to have several advantages[56-59] including: (1) shorter reaction time; (2) easiness to tune compositions of the products; and (3) more uniform product dimensions and composition. Zhang *et al.*[60] demonstrated the microwave assisted solvothermal route for the synthesis of BiOBr photocatalyst with strong adsorption, and excellent properties, using Bi $(NO_3)_3.5H_2O$, cetyltrimethylammonium bromide (CTAB) as bromine source, and diethylene glycol as solvent.

Carbon materials have been reported as efficient electron transport matrices. Song *et al.*[1] reported a green single step microwave assisted strategy for the synthesis of BiOBr and BiOBr/graphene composites. According to them, microwave irradiation helps in selective activation of the target precursors to initiate nucleation and subsequent growth.

4.3. Present work

The most effective and simple strategy to improve the photocatalytic activity of a photocatalyst is the construction of heterostructure by coupling of two semiconductor photocatalysts, as it provides a feasible method to promote the separation of photogenerated electron-hole pairs, and also combining of two semiconductors with different band gaps is flexible for broadening the visible light absorption.[61] P-n heterostructures with n- type $ZnFe_2O_4$ and p-type BiOBr were synthesized by Kong *et al.*[61] *via* simple ultrasound deposition method. The introduction of $ZnFe_2O_4$ into BiOBr lead to the considerable extension of absorption edge of BiOBr, and the composite showed exceptional VLD photocatalytic activity. Similarly, many other coupled systems concerned BiOBr such as BiOCl/BiOBr,[62] Ag/AgBr/BiOBr,[63] $(BiO)_2CO_3$/BiOBr,[64] and AgBr/BiOBr[65] have been reported to have higher photocatalytic performance than individual BiOBr. Many other materials, such as Ag,[66] Fe,[33] or g-C_3N_4[67] have been coupled with BiOBr to enhance the photocatalytic activity of BiOBr. All these above

mentioned literature reports motivated us to fabricate Ag_3PO_4/BiOBr heterojunctions with a hope of enhanced catalytic performance.

Ag_3PO_4 is a visible light responsive photocatalyst, and exhibits extremely high photooxidative capability for O_2 evolution from water, and decomposition of organic dyes.[68,69] Unfortunately, pure Ag_3PO_4 has low structural stability which limits its environmental applications.[70] Ag_3PO_4 has been previously coupled with many semiconductors to improve their catalytic efficiency such as Ag_3PO_4/TiO_2,[71] Ag_3PO_4/BiOI,[72] Ag_3PO_4/CeO_2,[70] Ag_3PO_4 loaded Bi_2MoO_6,[73] Ag_3PO_4/MoS_2,[74] $Ag_3PO_4/BiPO_4$,[75] Ag_3PO_4/SnO_2,[76] Ag_3PO_4/WO_3,[77] CdS@Ag_3PO_4,[78] Ag_3PO_4/ZnO,[79] and Ag_3PO_4/BiOCl.[80] To the best of our knowledge, no significant effort has been made for the preparation of Ag_3PO_4/BiOBr. The reason why we choose Ag_3PO_4 to couple with BiOBr is based on following considerations: (a) Ag_3PO_4 has a band gap of around 2.36-2.40 eV[68,69,81] which enables it to absorb visible light up to 540 nm, and therefore can act as a sensitizer, and enhance the visible light absorption. (b) Considering the low structural stability of pure Ag_3PO_4 and its unique photo oxidative ability, coupling of Ag_3PO_4 with BiOBr could be a good strategy to develop efficient and stable photocatalyst.

Therefore, herein an effective yet simple co-precipitation method has been reported to synthesize novel Ag_3PO_4/BiOBr heterojunction photocatalyst, and its photocatalytic activity was explored by decomposing refractory dye Rhodamine B. Various characterization techniques were used to study the structure, morphology, and optical properties of these heterojunctions. The photocatalytic experiment was performed in an immersion well reactor. The as synthesized composite system exhibited very high visible light induced photocatalytic activity. Scavenger experiments were carried out to investigate the primary reactive species involved in the photo decolourization of dye. Mineralization extent of dye was investigated by Chemical oxygen Demand (COD) technique. Photoluminescence (PL) analysis was used to confirm the effective separation of photoinduced charge carriers. The stability of the photocatalyst was investigated by repetition experiments.

4.4. Experimental

4.4.1. Preparation of BiOBr microspheres

The BiOBr microspheres were synthesized by simple precipitation method. 0.01 mol of $Bi(NO_3)_3.5H_2O$ was dissolved in absolute ethanol. Subsequently, NaBr aqueous solution (molar ratio of Bi/Br = 1:1) was added drop wise, and pH of the resultant suspension was adjusted to 8 using 1.5 M aqueous ammonia solution. The resulting mixture was stirred

for 12 h at 85 °C. Finally, the product was separated by centrifugation, washed with deionized water and absolute ethanol, and then dried at 80 °C for 10 h.

4.4.2. Preparation of Ag_3PO_4/BiOBr heterostructures

For the preparation of Ag_3PO_4/BiOBr heterostructures, 1.0 g of BiOBr was dispersed in 20 mL of water by ultrasonication, and different quantities of $AgNO_3$ and Na_3PO_4 were added into the suspension, and stirred for 6 h at room temperature. Subsequently, the Ag_3PO_4/BiOBr microspheres were separated by centrifugation, and washed with deionized water followed by absolute ethanol, and then vacuum dried at 80 °C for 10 h. The samples with different Ag/Bi weight ratio of 0.1, 0.3, 0.5, 0.7, and 0.9 were noted as AB1, AB3, AB5, AB7, and AB9, respectively. For comparison, pure Ag_3PO_4 powders were prepared by referring to previous studies.[82]

4.4.3. Characterization

The phase purity and the structural properties of the obtained samples were examined at room temperature by X-ray diffraction (XRD) using Shimadzu XRD-6100 X-ray diffractometer with Cu Kα radiation (λ=1.5406 A^o) and a scanning speed of 10^o/min in the 2θ ranges from 10^o to 80^o. The morphology was probed by Carl-Zeiss field-emission scanning electron microscope (FESEM) on which elemental analysis was also probed using EDS attachment. Transmission electron microscopy (TEM) studies were recorded on a TEM (JEM 2100F) instrument. The specific surface area was calculated by measuring N_2 adsorption and desorption isotherms on a Belsorp-Max and Belsorp-Aqua Porosimeter. UV-vis-NIR spectrophotometer (Perkin Elmer) equipped with an integrating sphere assembly was used to obtain UV-vis diffuse reflectance spectra (DRS) of the samples in the region of 300-800 nm. Flourospectrometer was used to obtain the photoluminescence spectra (PL) of the samples.

4.4.4. Photocatalytic activity test and Chemical Oxygen Demand (COD) measurements

The visible light photocatalytic activities of pure BiOBr, Ag_3PO_4, and Ag_3PO_4/BiOBr hybrids were evaluated by the photocatalytic degradation of Rhodamine B (RhB) dye and phenol aqueous solutions. The photocatalytic tests were performed in an immersion well photoreactor (consisting of inner and outer jacket) made of pyrex glass equipped with a magnetic bar, a water circulating jacket, and an opening for molecular oxygen. Visible light halogen linear lamp (500 W, 9500 Lumens) was used to carry out irradiations. The reaction temperature was kept constant at 20±0.3 ^oC using refrigerated circulating liquid bath. Prior to the illumination, the suspension containing 100 mL of dye with appropriate quantity of the catalyst (1 gL^{-1}) was magnetically stirred, while the solution was purged

continuously with atmospheric air for at least 30 min. in the dark to attain adsorption-desorption equilibrium between photocatalyst and pollutant. 5mL of sample suspensions were collected at 3 min. interval, centrifuged, and then analysed with (Shimadzu UV-Vis 1601) spectrophotometer. The change in absorbance of the dye was followed at its λ_{max} (554 nm) as a function of irradiation time. The observed absorbance is proportional to Beer-Lambert Law in the range of studied dye concentration. The concentration of dye was calculated by standard calibration curve obtained from the absorbance of the dye at different known concentrations. To investigate the effect of relevant reactive oxygen species, appropriate quantity of various quencher species were added in the reaction system in a manner similar to the photocatalytic experiment. The dosage of quenchers was referred to the previous studies.[83,84] COD was estimated before and after the irradiation in accordance with standard APHA method.[85,86]

4.5. Results and discussion

4.5.1. Structural characterization

Fig. 4.1 shows the XRD patterns of pure BiOBr, Ag_3PO_4, and Ag_3PO_4/BiOBr microspheres. All the detectable peaks in pure BiOBr can be assigned to the tetragonal primitive crystal structure of BiOBr.[87] The characteristic peaks of Ag_3PO_4 are in good accordance with the body centred cubic structure of Ag_3PO_4.[82] The Ag_3PO_4/BiOBr hybrids exhibit a coexistence of Ag_3PO_4 and BiOBr phases, with diffraction peaks corresponding to both Ag_3PO_4 and BiOBr. For all the composites the intensity of Ag_3PO_4 diffraction peaks increases with increase in its content.

The crystallite sizes of pure BiOBr and composite catalysts were calculated by the Scherer formula[41] (**Equation 4.1)**

$$D = K\,\lambda\,/\beta\cos\theta_B \qquad [4.1]$$

Where D is taken as crystallite size, K is a constant, β is the FWHM measured in radians on the 2θ scale, and θ_B is the Bragg angle for diffraction peaks. The crystallite sizes of pure BiOBr and composite catalysts are given in **Table 4.1**. It can be inferred from the **Table 4.1**, that the loading of Ag_3PO_4 does not affect the crystallite size of BiOBr microspheres.

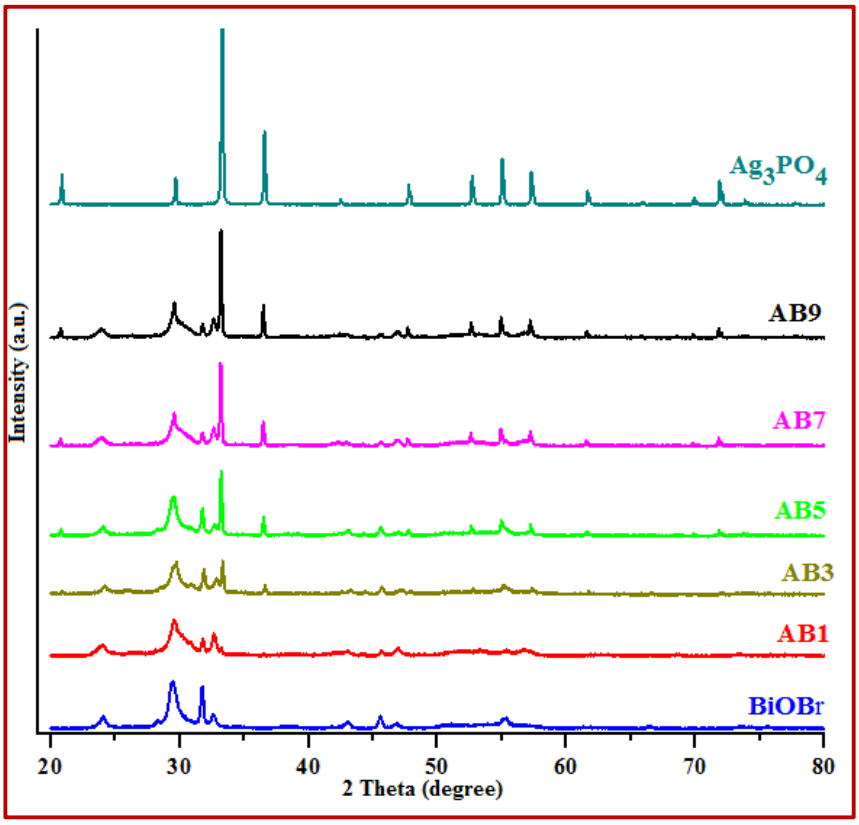

Fig. 4.1: XRD patterns of: BiOBr, AB1, AB3, AB5, AB7, AB9, and Ag_3PO_4.

Table 4.1. Crystallite size of pure and hybrid composites.

Sample	Crystallite Size (nm)
BiOBr	16.49
AB1	14.61
AB3	14.63
AB5	17.95
AB7	19.21
AB9	18.91

4.5.2. Morphological characterization

The detailed morphology and composition of Ag_3PO_4/BiOBr were investigated by SEM and EDS, as shown in **Fig. 4.2** and **Fig. 4.3**, respectively. The SEM image in **Fig. 4.2 (a)** shows that the pure BiOBr is made up of flower shaped microspheres with smooth surfaces. **Fig. 4.2 (b-f)** presents the SEM images of Ag_3PO_4/BiOBr hybrids. The

morphology of BiOBr and Ag_3PO_4/BiOBr hybrids is similar except for small Ag_3PO_4 particles formed on the surface of BiOBr.

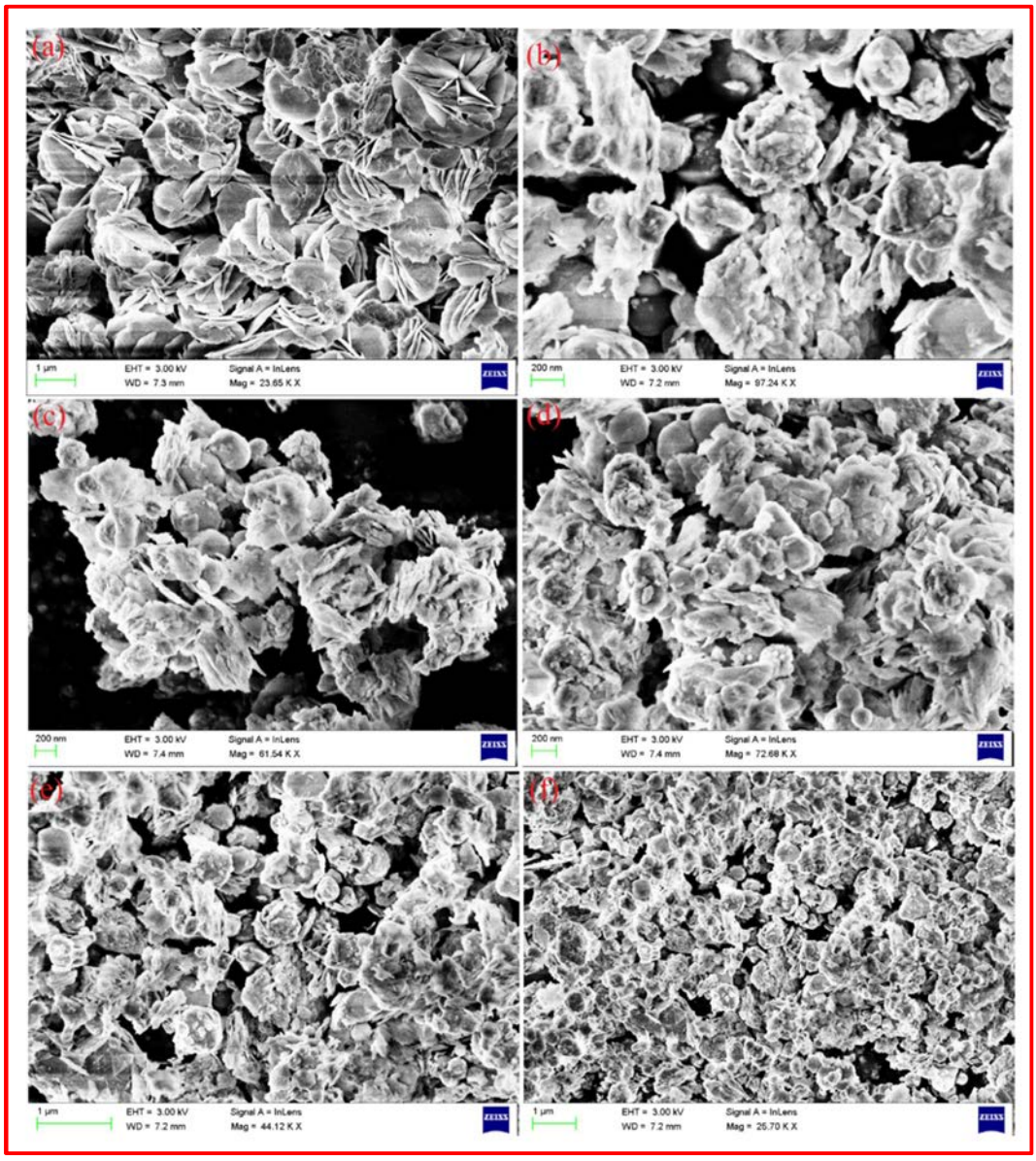

Fig. 4.2: SEM images of: (a) BiOBr, (b) AB1, (c) AB3, (d) AB5, (e) AB7, and (f) AB9.

Because, it is not clear to distinguish between BiOBr and Ag_3PO_4/BiOBr hybrids, EDS spectrum of BiOBr and hybrids was collected, and is shown in **Fig. 4.3**. The EDS spectrum of pure BiOBr **(Fig. 4.3 (a))** shows the presence of Bi, O, and Br elements whereas the hybrids **(Fig. 4.3 (b-f))** show the presence of Ag and P in addition to Bi, O, and Br elements. Further, with increase in content of Ag_3PO_4, the amount of Ag and P as detected by EDS also increases. This clearly proves the formation of Ag_3PO_4 particles. Moreover, the Ag/Bi weight ratios in hybrids

obtained from EDS results is virtually identical or very close to the theoretical Ag/Bi ratios. All these results clearly prove the formation of Ag_3PO_4 in hybrids.

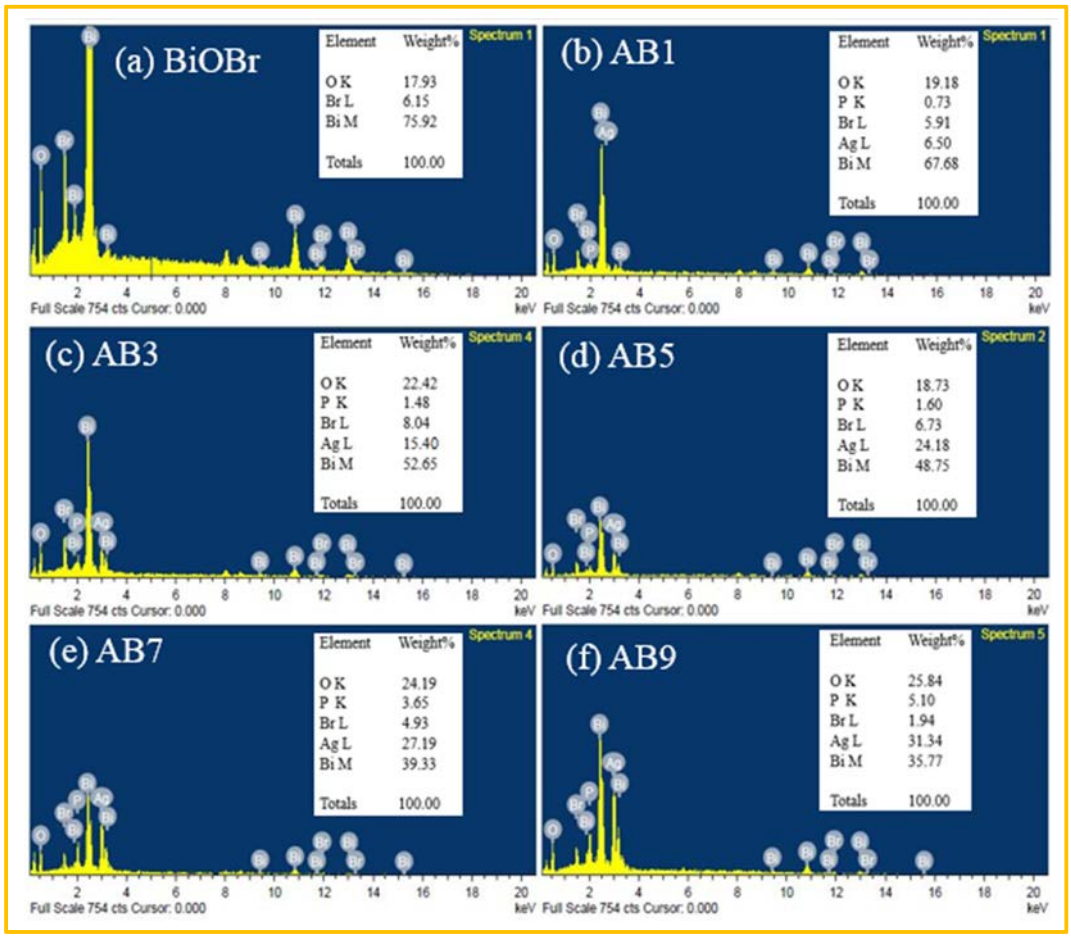

Fig. 4.3: EDS spectrum of: (a) BiOBr, (b) AB1, (c) AB3, (d) AB5, (e) AB7, and (f) AB9.

TEM was used to further investigate the structure and morphology of the sample. The TEM image of pure BiOBr microsphere **(Fig. 4.4 (a))** shows that it has a spherical structure with smooth surface, whereas that of Ag_3PO_4/BiOBr hybrid **(Fig. 4.4 (b))** depicts lot of subtle Ag_3PO_4 particles grown on the surface of BiOBr microspheres indicating the formation of composite.

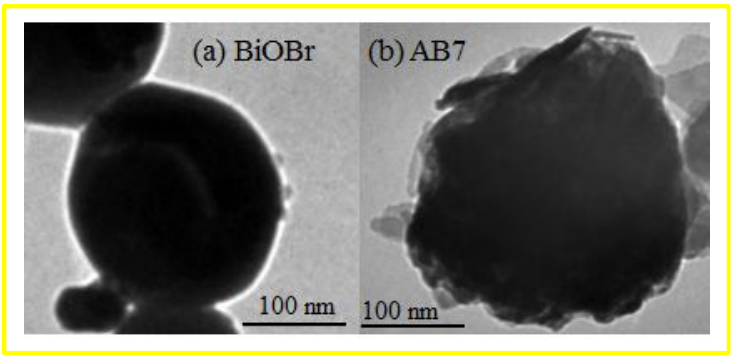

Fig. 4.4: TEM images of the samples: (a) BiOBr, (b) AB7.

4.5.3. FTIR Study

Fig. 4.5 displays the FT-IR spectrum of BiOBr and Ag_3PO_4/BiOBr composite (AB7). The band at 1627 cm^{-1} in the spectrum of BiOBr is attributed to OH stretching vibrations of water molecule. The absorption band at 522 cm^{-1} is ascribed to the Bi–O stretching mode. The absorption bands at 1022 cm^{-1}, 1070 cm^{-1}, and 550 cm^{-1} in the spectrum of Ag_3PO_4/BiOBr (AB7) correspond to the P-O stretching vibrations of PO_4^-.[88]

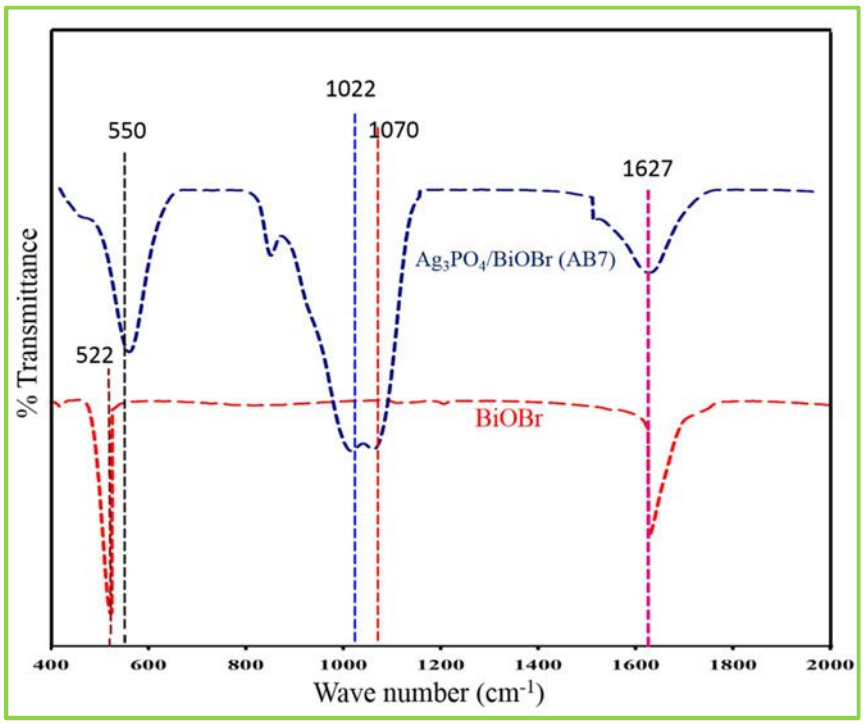

Fig. 4.5: FTIR spectra of BiOBr and AB7.

4.5.4. *BET analysis*

Fig. 4.6 presents the N_2 adsorption-desorption isotherms of pure BiOBr and AB7 respectively. According to IUPAC classification, both BiOBr and AB7 exhibit type III isotherms. Both BiOBr and AB7 in the low pressure region have quite gentle curves. With increase in P/P_o, the adsorption increases slowly and show a sudden jump around 0.9-1.0, which may be attributed to the capillary condensing phenomenon of N_2 in the mesoporous pressure region. The curves of both BiOBr and AB7 are similar indicating that the morphology and pore size of both these samples is more or less identical. The Brunauer–Emmett–Teller (BET) surface area of AB7 (35.30 m^2g^{-1}) was found to be higher than BiOBr (15.8 m^2g^{-1}) which may be beneficial in reducing the electron-hole recombination.

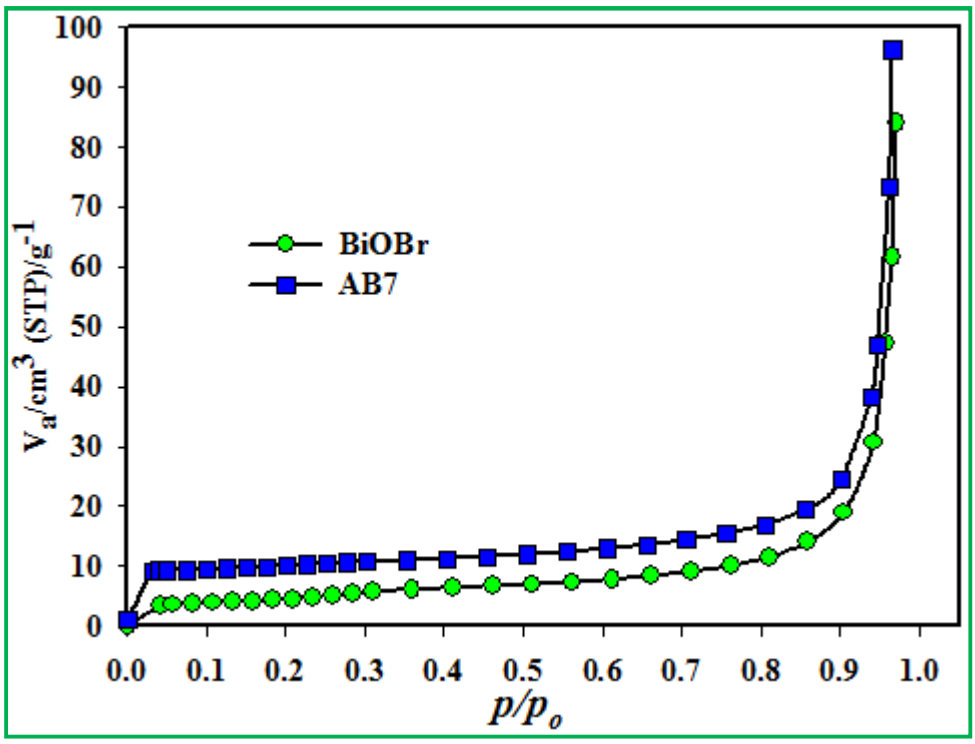

Fig. 4.6: Nitrogen adsorption–desorption isotherms for BiOBr and AB7.

4.5.5. DRS

The optical absorbance of obtained samples was measured by UV–vis. diffuse reflectance spectra (DRS). As shown in the **Fig. 4.7**, BiOBr has an absorption edge around 430 nm, while Ag_3PO_4 has absorption edge around 520 nm. As can be seen from the figure, Ag_3PO_4/BiOBr composites have better visible light absorption compared to pure BiOBr, with AB7 having absorption edge around 503 nm. Therefore, light absorption of composites is enhanced to a large extent through the introduction of Ag_3PO_4.

As reported by the Butler,[89] the band gap energy of semiconductor is calculated by **Equation 4.2**.

$$(h\nu.\alpha) = (A h\nu - Eg)^{n\backslash 2} \qquad [4.2]$$

Since α is proportional to kubelka – munk function F(R), the expression becomes

$$h\nu.F(R) = (A h\nu - Eg)^{n\backslash 2} \qquad [4.3]$$

where *h* is planck's constant, *v* is the light frequency, F(R) is the kubelka–munk function, A is the proportional constant, and Eg is the Band gap energy. The value of 'n' is determined by the type of optical transition (n=1 for direct transition and n = 4 for indirect transition). From the experimental data, the Eg of BiOBr and Ag_3PO_4 were determined from the plot of $(F(R).\ h\nu)^{1/2}$ *vs.* $h\nu$ **(Fig. 4.8 (a))** and $(F(R).\ h\nu)^2$ *vs.* $h\nu$ **(Fig. 4.8 (b))** respectively. The band gaps for BiOBr and Ag_3PO_4 were estimated to be 2.74 eV and 2.36 eV respectively.

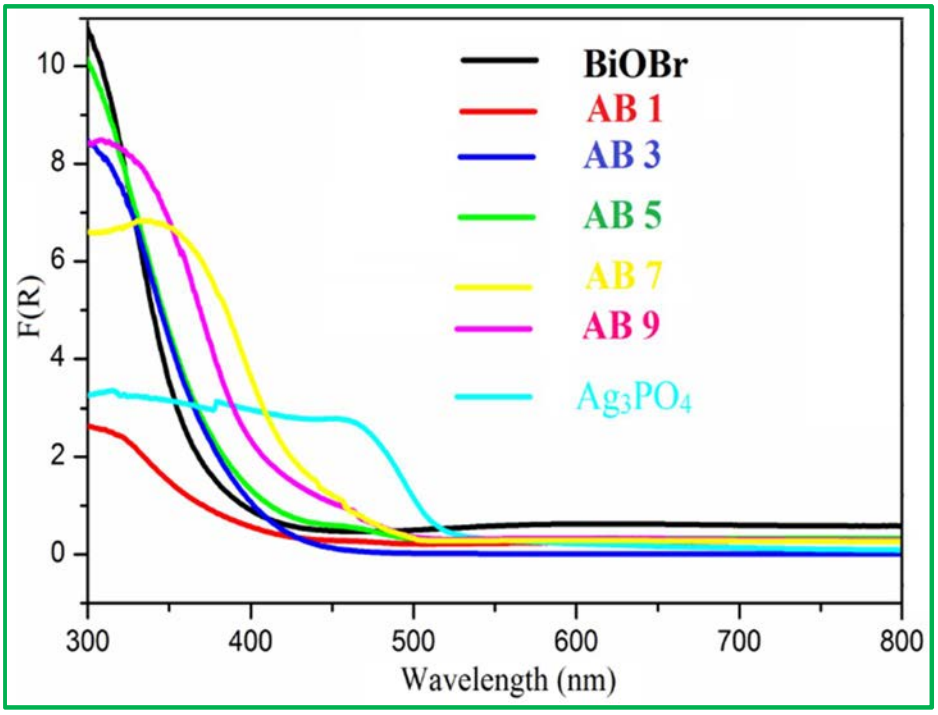

Fig. 4.7: DRS of BiOBr and Ag_3PO_4/BiOBr hybrids.

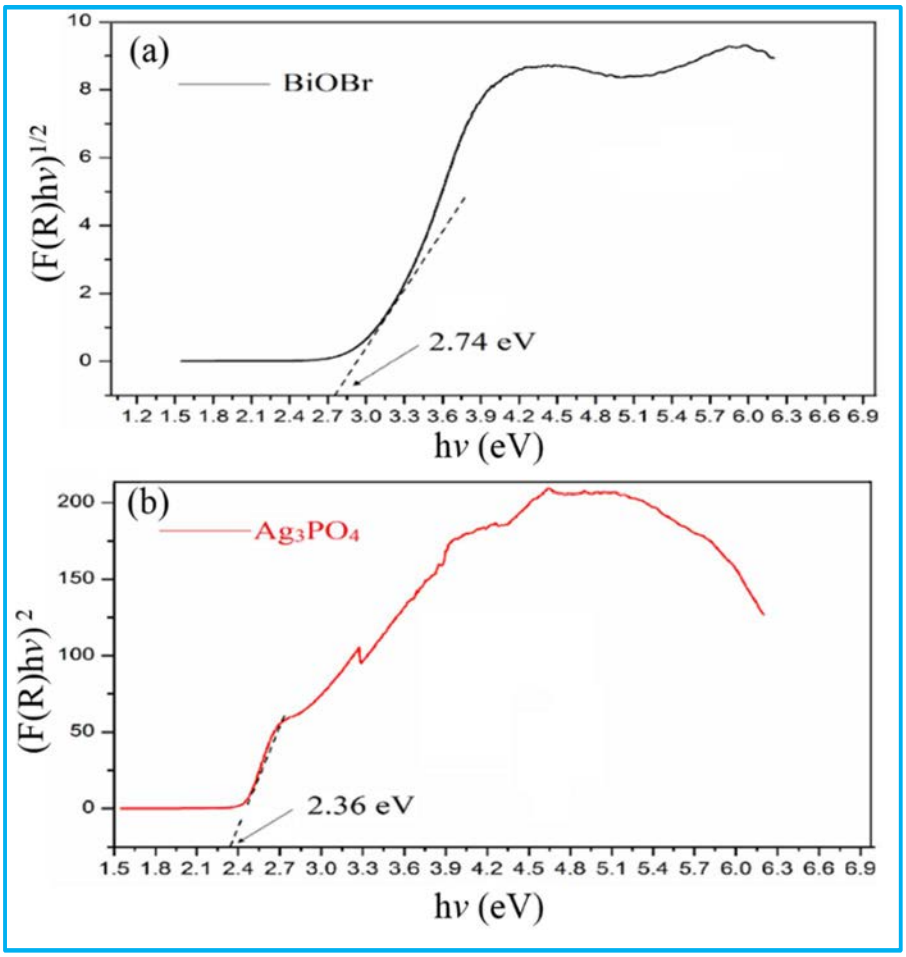

Fig. 4.8: (a) Plot of $(F(R).h\nu)^{1/2}$ versus energy ($h\nu$) for the band gap energy of BiOBr, and (b) $(F(R).h\nu)^{2}$ versus energy ($h\nu$) for Ag_3PO_4.

4.5.6. PL spectra

The activity of a photocatalyst, and the subsequent quantum yield of the reaction are largely determined by the life time of the electron-hole pairs.[90] Since the electron-hole recombination is mainly responsible for PL emissions, therefore, the PL spectra was used to investigate the recombination of photoinduced charge carriers.[91,92] The low intensity of PL emission implies the lower rate of recombination of photoinduced charge carriers.[93] **Fig. 4.9** presents the PL spectra of BiOBr, Ag_3PO_4, and AB7. The BiOBr shows only one emission peak centred around 435 nm, whereas Ag_3PO_4 shows two emission peaks centred around 480 nm and 550 nm. AB7 presents the lowest emission peaks centred around 437 nm and 540 nm suggesting that the electron-hole recombination is lowest in AB7 which results into the weak intensities of PL emissions in AB7, compared with pure BiOBr and Ag_3PO_4. The most probable reason for this kind of behaviour is the effective separation of photoinduced charge carriers in AB7 as a result of heterojunction.

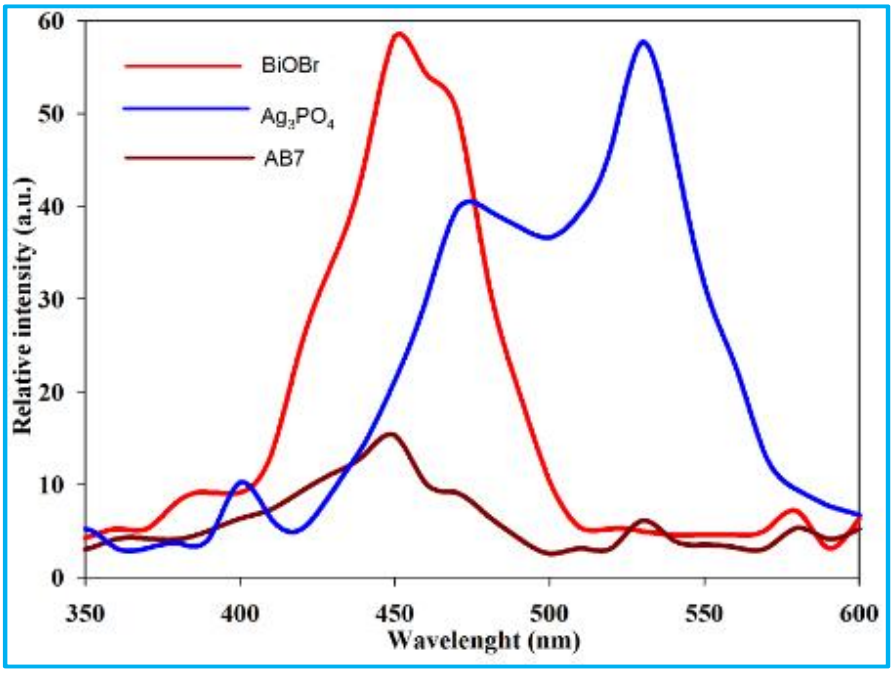

Fig. 4.9: PL spectra of the samples (λ_{exc} = 400 nm).

4.5.7. Photocatalytic properties

The photocatalytic activities of the as prepared Ag_3PO_4/BiOBr samples were evaluated by the degradation of RhB under visible light irradiation. **Fig. 4.10 (b)** presents the variations of the RhB concentration (C_t/C_o) over different samples as a function of irradiation time. Prior to the irradiation, the dark adsorption was checked for 30 minutes. As can be seen from the **Fig. 4.10 (b)**, the adsorption is almost insignificant, and hence can be neglected. **Fig. 4.10 (b)** shows that all Ag_3PO_4/BiOBr hybrids exhibit higher photocatalytic

activities, compared to pure BiOBr and Ag_3PO_4. The photocatalytic activities of composites enhance with increasing amounts of Ag_3PO_4. Among the heterojunctions, the highest photocatalytic activity is achieved for AB7 with nearly 97.5 % of RhB removal after 21 min. of visible light irradiation. The two important factors responsible for the enhanced visible light activity of heterojunctions are: (a) increased surface area of the composites which prevents the electron-hole recombination, and (b) the formation of heterojunction with natural energy bias which facilitates the transfer of photoinduced charge carriers, and hence impedes the electron-hole recombination. The photocatalytic activity of the composites is related to the amount of Ag_3PO_4 loading, and the activity sequence is in the order: AB7 > AB9 > AB5 > AB3 > AB1 > BiOBr > Ag_3PO_4. **Fig. 4.10 (a)** depicts the change in visible spectrum of RhB solution at different time intervals of irradiation using the hybrid AB7 as photocatalyst.

It is well known that the photocatalytic decolourization of most of the dyes follow pseudo- first order kinetics model,[94] and therefore, to understand the reaction kinetics of RhB degradation, the apparent pseudo-first order kinetics model given by **Equation 4.4**, was applied in experiments.

$$\ln(C_o/C_t) = K_{app}t \qquad [4.4]$$

Where K_{app} is apparent pseudo first order rate constant. The values of K_{app} for all the composites were calculated *via* the first order linear fit from the data of **Fig. 4.10 (c),** and are given in **Table 4.2**. The value of K_{app} increases with increase in the content of Ag_3PO_4, and the highest K_{app} is observed for AB7 composite. The degradation constant of AB7 (0.17 min^{-1}) is found to be about 3.81 times that of BiOBr (0.0446min^{-1}), and 5.24 times that of Ag_3PO_4 (0.0324 min^{-1}).

Table 4.2: Pseudo-first order rate constants (K_{app}) of different photocatalysts for the decolourization of RhB calculated from the plots of ln (C_o/C_t) versus irradiation time.

Sample	$K_{app}(min^{-1})$
BiOBr	0.0446
Ag_3PO_4	0.0324
AB1	0.0594
AB3	0.0691
AB5	0.0924
AB7	0.1700
AB9	0.1212

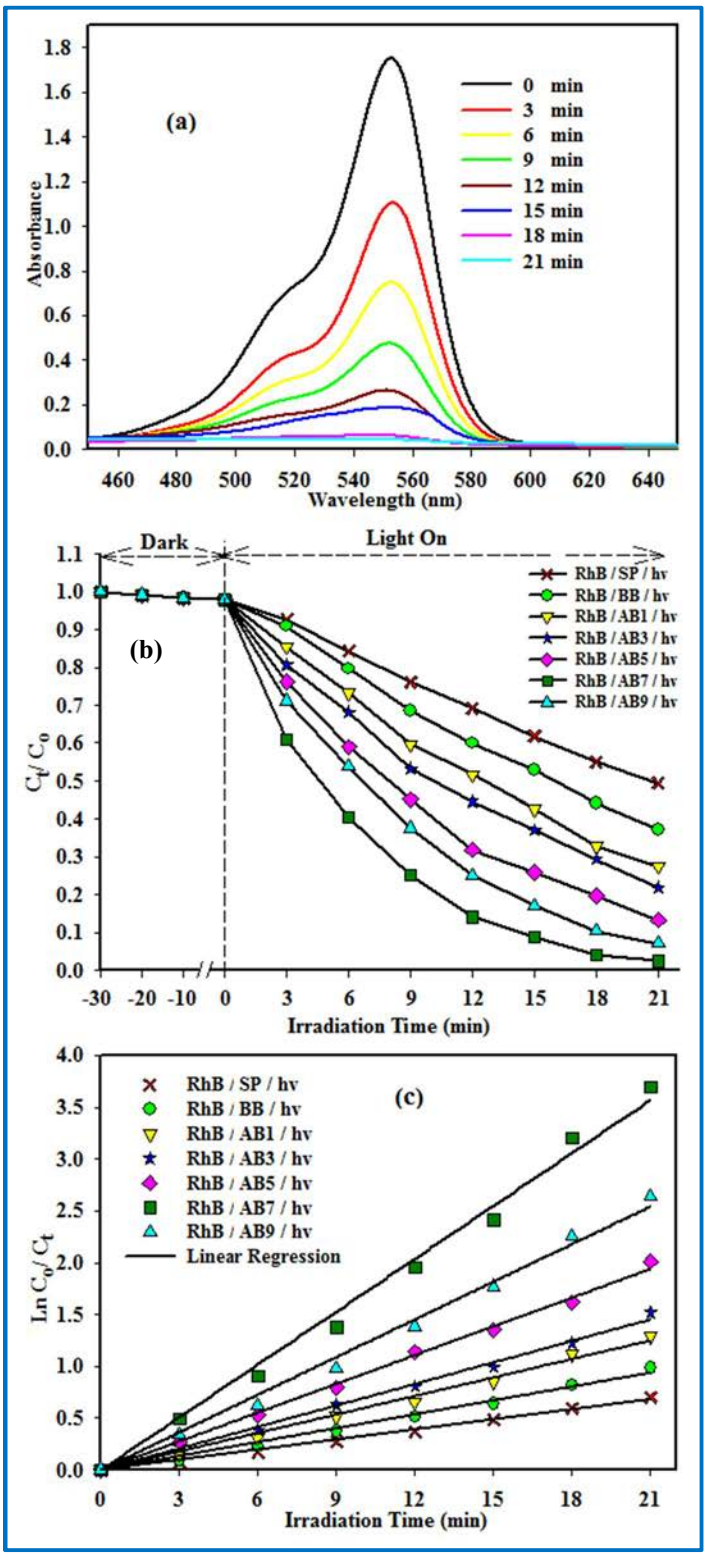

Fig. 4.10: (a) Change in UV-vis spectra of RhB aqueous suspension in the presence of AB7 at different irradiation times, (b) Change in concentration (C_t/C_o) of RhB in the presence of Ag_3PO_4, BiOBr, and Ag_3PO_4/BiOBr hybrids under visible light, and (c) $\ln(C_o/C_t)$ versus irradiation time for different catalysts.

To further confirm the mineralization, the COD removal during the photocatalytic reaction was carried out in accordance with standard APHA method.[85,86] The decrease in the value of COD signifies the extent of mineralization of organic species. As shown in the **Fig. 4.11**, the COD value decreases substantially with irradiation time. After 21 minutes the COD is reduced to about 96% of initial value. The photodegradation efficiency was calculated by the **Equation 4.5**.

$$\text{Efficiency}(\%) = \frac{Initial(\ COD) - Final\ (COD)}{Initial\ (COD)} \times 100 \qquad [4.5]$$

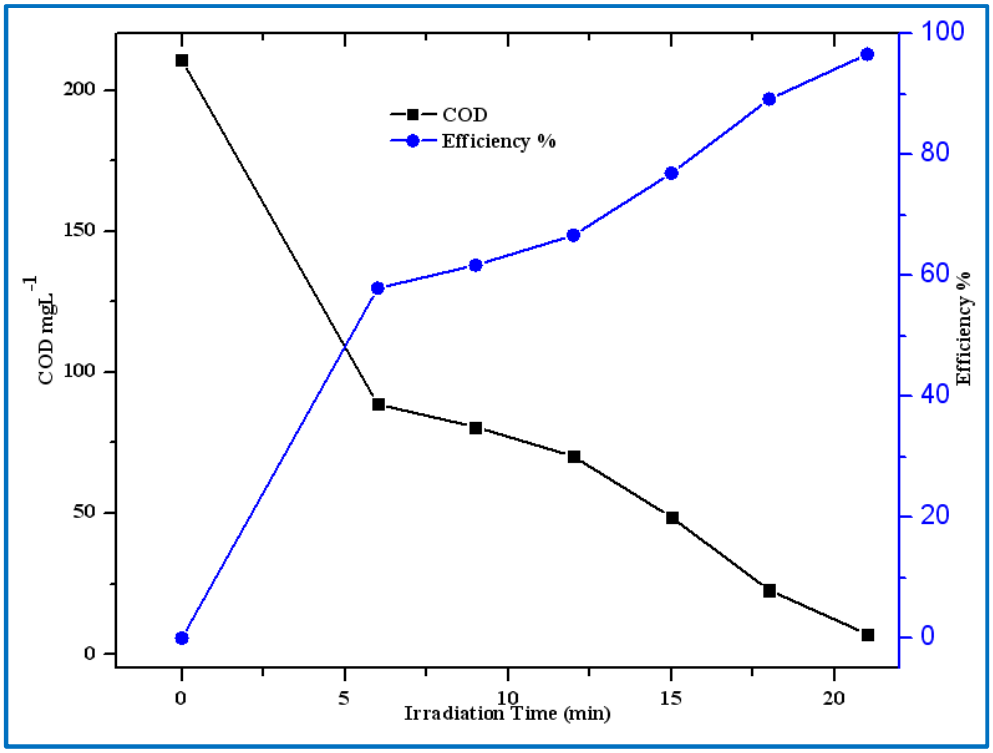

Fig. 4.11: Variation of COD with irradiation time and percent (%) efficiency.

The photocatalytic activity of as prepared Ag_3PO_4/BiOBr heterojunctions was compared to the previously reported visible light activity of various BiOBr heterojunctions,[33,62,95-98,] as shown in **Table 4.3**. From **Table 4.3**, it is clear that the Ag_3PO_4/BiOBr heterojunctions show enhanced visible light activity compared to the previously reported other heterojunctions.

Table 4.3. Visible light percent (%) decolourization of RhB over previously reported BiOBr heterojunctions and Ag_3PO_4/BiOBr heterojunction.

S. No	Catalyst	% Decolourization of RhB	Irradiation Time (min)	Reference
1	MoS_2 coupled BiOBr	100 %	170	[95]
2	BiOBr/ montmorillonite	98.96%	120	[96]
3	BiOBr/Fe_2O_3	97.8%	120	[97]
	BiOBr/Fe_3O_4	100%		
4	BiOCl-BiOBr	99%	60	[62]
5	Fe- doped BiOBr	73 %	30	[33]
6	BiOBr-C_3N_4	100%	40	[67]
7	Ag Modified BiOBr	100%	40	[66]
8	BiOBr-TiO_2	100%	20	[98]
9	Ag_3PO_4/BiOBr	97.5%	21	

4.5.8. Discussion of Degradation mechanism

4.5.8.1. Formation of reactive species

Various scavengers of the reactive species were added to the reaction system to investigate the type of reactive species (such as $^{\bullet}OH$, h^+, H_2O_2 and $^{\bullet}O_2^-$) produced, and contribute maximum towards the decolourization of RhB during the photocatalytic process. Benzoquinone (BQ) was added as a superoxide radical ($O_2^{-\bullet}$) scavenger, ammonium oxalate (AO) as h^+, and tert-butylalcohol (TBA) as a hydroxyl radical ($^{\bullet}OH$) scavenger.[82-84,99,100] As shown in the **Fig. 4.12**, AO and TBA inhibits the removal efficiency of RhB and the K_{app} value decreases significantly, indicating that h^+ and $^{\bullet}OH$ are the primary reactive species in the photodegradation process of RhB using Ag_3PO_4/BiOBr composite. The addition of BQ in the reaction system has no obvious effect on the photodegradation process of RhB and K_{app} value, suggesting that $O_2^{-\bullet}$ is not the primary reactive species in the photocatalytic degradation process of RhB.

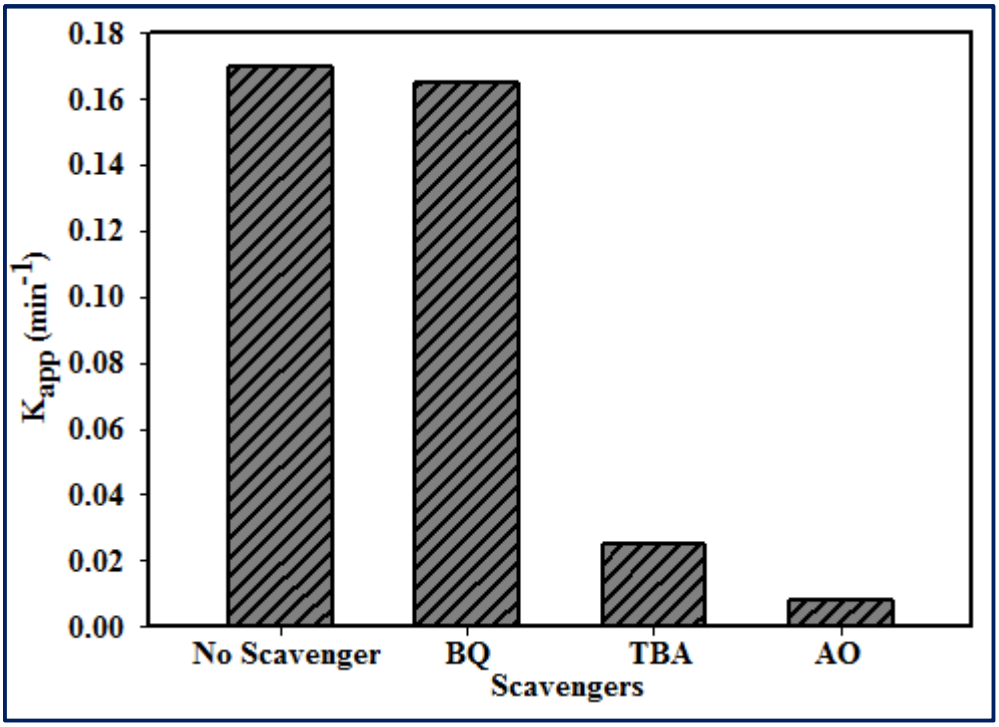

Fig. 4.12: Effect of scavengers on decolourization of RhB over AB7; BQ=Benzoquinone, TBA=tert-butylalcohol, AO=ammonium oxalate.

4.5.8.2. Origin of reactive species

Photocatalytic mechanism and photosensitization are the two possible reaction mechanisms responsible for the origin of reactive species. Phenol, which is visible light inactive, was used as a model pollutant to ensure that the reactive species originate from the photocatalytic process of the Ag_3PO_4/BiOBr, and not from the sensitization of dye under visible light irradiation. Fig. **4.13 (a)** presents the variations of the phenol concentration (C_t/C_o) over BiOBr, Ag_3PO_4, and AB7 samples as a function of irradiation time. Prior to the irradiation, dark adsorption was checked for 30 min and was found to be negligible. **Fig. 4.13 (a)** displays that concentration of phenol decreases slightly with increasing irradiation time in presence of pure Ag_3PO_4 and BiOBr, whereas there is a sharp decrease in the concentration of phenol in presence of AB7. The values of K_{app} for the degradation of phenol in the presence of BiOBr, Ag_3PO_4, and AB7 were calculated *via* the first order linear fit from the data of **Fig. 4.13 (b)**. The value of K_{app} for AB7 (0.0957 min^{-1}) is found to be 3.5 times higher than that of BiOBr (0.0272 min^{-1}) and 5.5 times higher than that of Ag_3PO_4 (0.0174 min^{-1}). These results clearly indicate that the reactive species originate from the photocatalytic process of the Ag_3PO_4/BiOBr composites under visible light, and rules out the possibility of photosensitization by dye molecules.

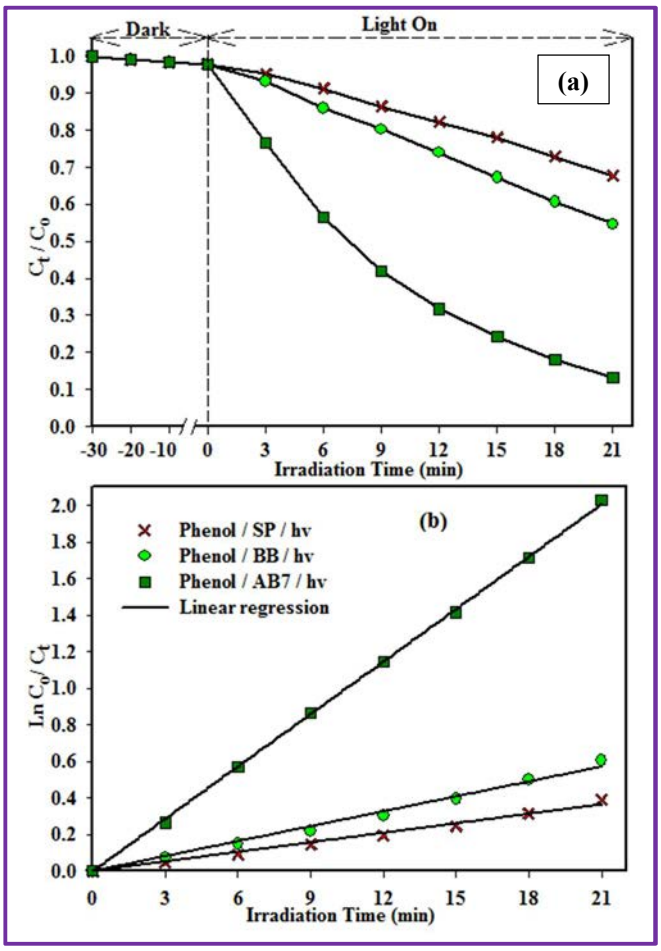

Fig. 4.13: (a) Change in concentration (C_t/C_o) of phenol in the presence of BiOBr, Ag_3PO_4 and AB7 (b) Phenol degradation curves of ln (C_o/C_t) versus irradiation time for BiOBr, Ag_3PO_4 and AB7.

4.5.8.3. Possible photocatalytic mechanism

The photocatalytic activity of a heterojunction in a hybrid semiconductor is directly related to the electronic band structure of individual components and the fate of the photoinduced charge carriers.[101] To fully understand the photocatalytic mechanism, the band edge position of the valence band and the conduction band of Ag_3PO_4 and BiOBr was determined by using the empirical **Equation 4.6**.[29]

$$E_{VB} = X - E_c + 0.5E_g. \qquad [4.6]$$

Where E_{VB} is the energy of VB edge potential, X is the electronegativity of semiconductor, and E_c is the energy of free electrons on hydrogen scale (4.5 eV). The top of the valence band E_{VB} of BiOBr and Ag_3PO_4 were calculated to be 3.05 eV/NHE and 2.63 eV/NHE, respectively. Moreover, the conduction band edge potential E_{CB} can be determined by **Equation 4.7**.

$$E_{CB} = E_{VB} - E_g. \qquad [4.7]$$

The E_{CB} for BiOBr and Ag_3PO_4 were elicited as 0.31 eV/NHE and 0.27 eV/NHE, respectively.

From the calculated E_{VB} and E_{CB}, we can draw a schematic diagram of band alignment of Ag_3PO_4/BiOBr, as shown in **Fig. 4.14**. BiOBr has more positive VB and CB than Ag_3PO_4 which results in the generation of natural energy bias at heterojunction, and subsequent transfer of photoinduced charge carriers.[102,103]

Under visible light irradiation, both Ag_3PO_4 and BiOBr generate electron-hole pairs. As shown in the **Fig. 4.14**, the photoexcited electrons on the less positive CB of Ag_3PO_4 will prefer to flow down to the more positive CB of BiOBr, while the photogenerated holes on the more positive VB of BiOBr will transfer to the less positive VB of Ag_3PO_4. This leads to the efficient separation of electron-hole pairs, and thus prolonged life of photoinduced charge carriers.

Although, the photogenerated electrons are capable of reducing O_2 to O_2^-, but since the CB potential of BiOBr semiconductor is less negative than the standard reduction potential of oxygen (- 0.046 eV),[104] sufficient potential cannot be generated by CB of BiOBr to reduce O_2 to O_2^-. Thus, O_2^- is not involved in decolourization process of RhB. At the same time the E_{VB} value of Ag_3PO_4 (2.63 eV) is more positive than the E^o ($^\bullet OH/H_2O$) = +2.27 eV), indicating that sufficient potential can be generated by h^+ on VB of Ag_3PO_4 to oxidize H_2O to $^\bullet OH$.[105]

Based on the above discussion, the mechanism for the photocatalytic degradation of RhB on Ag_3PO_4/BiOBr heterojunction may be proposed as described in **Equation 4.8-4.12**.

$$Ag_3PO_4/BiOBr + h\nu \longrightarrow Ag_3PO_4 (e^-_{CB} + h^+_{VB})/BiOBr (e^-_{CB} + h^+_{VB}) \quad (4.8)$$

$$Ag_3PO_4 (e^-_{CB}) + BiOBr \longrightarrow BiOBr (e^-_{CB}) \quad (4.9)$$

$$BiOBr (h^+_{VB}) + Ag_3PO_4 \longrightarrow Ag_3PO_4 (h^+_{VB}) \quad (4.10)$$

$$Ag_3PO_4 (h^+_{VB}) + H_2O \longrightarrow H^+ + {}^\bullet OH \quad (4.11)$$

$$^\bullet OH \; Ag_3PO_4 (h^+_{VB}) + RhB \longrightarrow Products \quad (4.12)$$

We propose that under visible light irradiation both Ag_3PO_4 and BiOBr are simultaneously excited and result into the formation of electron-hole pairs. The electrons from the CB of Ag_3PO_4 are injected into the CB of BiOBr, whereas holes from VB of BiOBr are injected into the VB of Ag_3PO_4. These holes on the VB of Ag_3PO_4 then combine with water and oxidize it into $^\bullet OH$. The $^\bullet OH$ radicals then react with RhB and decompose it into intermediate products. The mechanism is well supported by the results of DRS, PL studies, and the effect of scavengers.

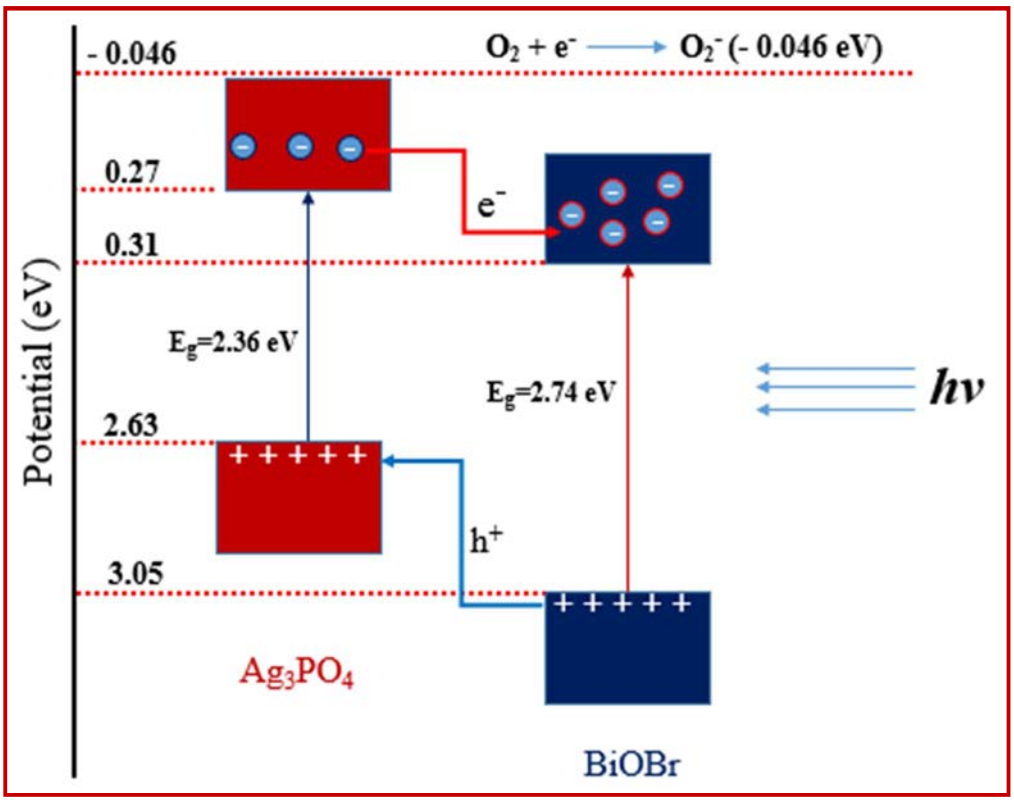

Fig. 4.14: Schematic diagram of electron-hole pair separation and the possible reaction mechanism over Ag_3PO_4/BiOBr photocatalyst under visible light irradiation.

4.5.9. Stability of catalyst

The stability of the silver based catalyst is always of vital consideration because there are fair chances of reduction of Ag^+ into Ag^o metal by the excited electrons.[70,82] Therefore, repeatability experiments of the RhB degradation over AB7 were taken to investigate the stability of the Ag_3PO_4/BiOBr catalyst. As shown in the **Fig. 4.15 (a)**, the degradation of RhB by AB7 is maintained at 95 % after 6 recycling runs suggesting that Ag_3PO_4/BiOBr has high stability under visible light irradiation. The XRD results of used AB7 after 6 recycling runs **(Fig. 4.15 (b))** reveals that the structure and the phase remains intact with no peak detection for Ag^o metal. Thus, reason for the stability of the catalyst is the efficient separation of photogenerated electron-hole pairs, and the fast transfer of excited electrons from the conduction band of Ag_3PO_4 to the conduction band of BiOBr.

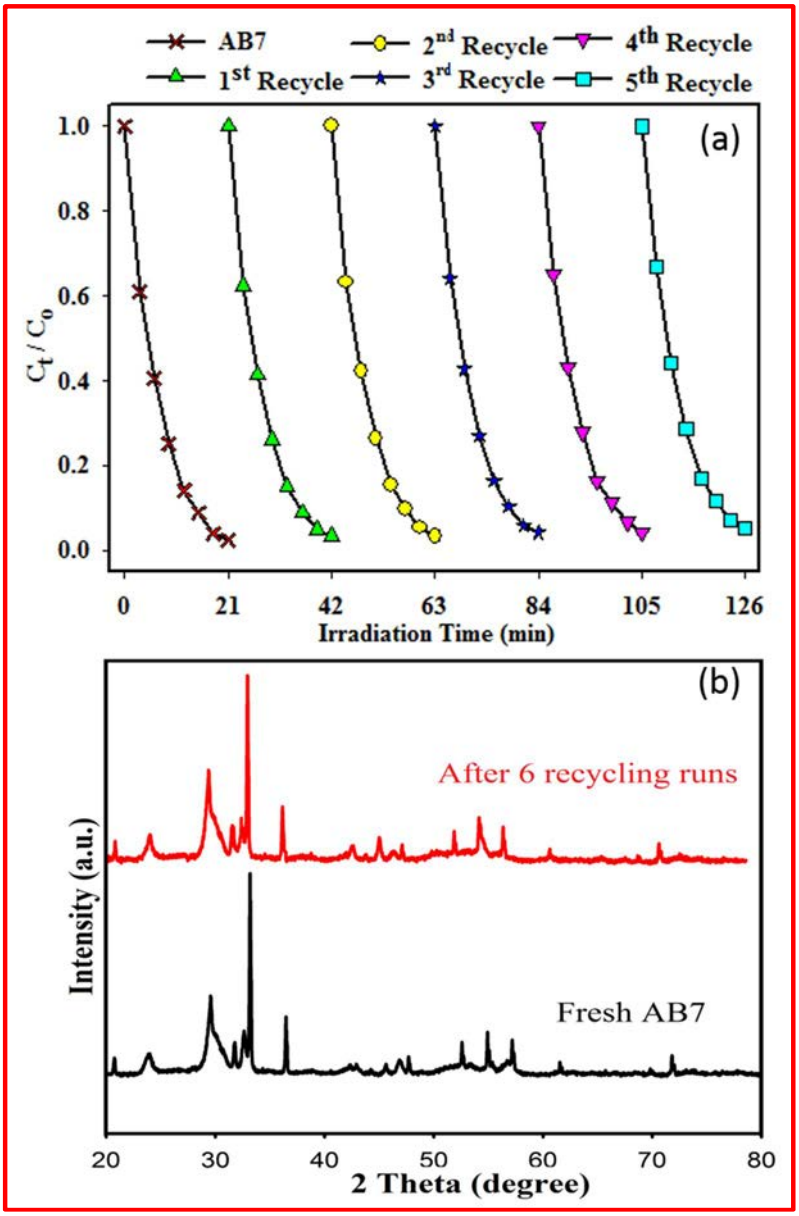

Fig. 4.15: (a) Cycling runs of AB7 for decolourization of RhB under visible light, (b) XRD patterns of Fresh AB7 and used AB7 after 6 recycling runs.

4.6. Conclusion

Efficient visible light active Ag_3PO_4/BiOBr microspheres were synthesized *via* simple co-precipitation method. The as prepared hybrids showed enhanced visible light absorption, and exhibited better photocatalytic activity on the degradation of RhB and phenol, compared to pure BiOBr and Ag_3PO_4 samples under visible light irradiation. The optimal content of Ag_3PO_4 in the Ag_3PO_4/BiOBr catalyst was found to be Ag/Bi weight ratio of 0.7. The photocatalytic activity did not show any significant decrease after 6 recycling runs. On the basis of experimental and theoretically calculated results, the reactive holes were suggested to play critical role in the photodegradation of RhB over the

Ag_3PO_4/BiOBr catalyst. Considering the facile and environment friendly route for the synthesis of Ag_3PO_4/BiOBr hybrids, and the enhanced visible light absorption of Bismuth Oxybromide due to the introduction of silver based compound, it is possible to widely apply these highly efficient Ag_3PO_4/BiOBr hybrids in various fields such as waste water treatment.

References

[1] S. Song, W. Gao, X. Wang, X. Li, D. Liu, Y. Xing and H. Zhang, *Dalton Trans.* **41** (2012) 10472.

[2] J. Zhang, F. J. Shi, J. Lin, D. F. Chen, J. M. Gao, Z. X. Huang, X. X. Ding and C. C. Tang, *Chem. Mater.* **20** (2008) 2937.

[3] H. Deng, J. W. Wang, Q. Peng, X. Wang and Y. D. Li, *Chem. Eur. J.* **11** (2005) 6519.

[4] D. Berlincourt, *J. Acoust. Soc. Am.* **91** (1992) 3034.

[5] R. W. Whatmore, *Rep. Prog. Phys.* **49** (1986) 1335.

[6] L. Li, L. Ai, C. Zhang and J. Jiang, DOI: 10.1039/c3nr06533b.

[7] M. Shang, W. Z. Wang, J. Ren, S. M. Sun, L. Wang and L. Zhang, *J. Hazard. Mater.* **19** (2009) 6213.

[8] X. P. Lin, F. Q. Huang, W. D. Wang and K. L. Zhang, *Appl. Catal.* A **307** (2006) 257.

[9] W. F. Yao, X. H. Xu, H. Wang, J. T. Zhou, X. N. Yang, Y. Zhang, S. X. Shang and B. B. Huang, *Appl. Catal. B* **52** (2004) 109.

[10] K. Zhu, N. R. Neale, A. Miedaner and A. J. Frank, *Nano Lett.* **7** (2007) 69.

[11] K. L. Zhang, C. M. Liu, F. Q. Huang, C. Zheng and W. D. Wang, *Appl. Catal. B* **68** (2006) 125.

[12] H. An, Y. Du, T. Wang, C. Wang, W. Hao and J. Zhang, *Rare Met.* **27** (2008) 243.

[13] X. P. Lin, T. Huang, F. Q. Huang, W. D. Wang and J. L. Shi, *J. Phys. Chem. B* **110** (2006) 24629.

[14] W. Wang, F. Huang and X. Lin, *Scr. Mater.* **56** (2007) 669.

[15] Z. H. Ai, W. K. Ho, S. C. Lee and L. Zhang, *Environ. Sci. Technol.* **43** (2009) 4143.

[16] C. H. Wang, C. L. Shao, Y. C. Liu and L. Zhang, *Scr. Mater.* **59** (2008) 332.

[17] W. L. Huang, *J. Comput. Chem.* **30** (2009) 1882.

[18] Y. F. Fang, Y. P. Huang, J. Yang, P. Wang and G. W. Cheng, *Environ. Sci. Technol.* **45** (2011) 1593.

[19] J. Xu, W. Meng, Y. Zhang, L. Li and C. S. Guo, *Appl. Catal. B* **107** (2011) 355.

[20] M. A. Gondal, X. F. Chang, M. A. Ali, Z. H. Yamani, Q. Zhou and G. B. Ji, *Appl. Catal. A* **397** (2011) 192.

[21] M. Shang, W. Z. Wang and L. Zhang, *J. Hazard. Mater.* **167** (2009) 803.

[22] A. K. Geim and K. S. Novoselov, *Nat. Mater.* **6** (2007) 183.

[23] S. Sharma, A. Ganguly, P. Papakonstantinou, X. P. Miao, M. X. Li, J. L. Hutchison, M. Delichatsios and S. Ukleja, *J. Phys. Chem. C* **114** (2010) 19459.

[24] L. S. Zhang, W. Z. Wang, Z. G. Chen, L. Zhou, H. L. Xua and W. Zhu, *J. Mater. Chem.* **17** (2007) 2526.

[25] H. L. Xu, W. Z. Wang and W. Zhu, *J. Phys. Chem. B* **110** (2006) 13829.

[26] K. Yu, S. Yang, H. He, C. Sun, C. Gu and Y. Ju, *J. Phys. Chem.* A **113** (2009) 10024.

[27] Z. Jiang, F. Yang, N. Luo, B. T. T. Chu, D. Sun, H. Shi, T. Xiao and P. P. Edwards, *Chem. Commun.* (2008) 6372.

[28] C. Yu, J. C. Yu, C. Fan, H. Wen and S. Hu, *Mater. Sci. Eng. B* **166** (2010) 213.

[29] X. Zhang, L. Zhang, T. Xie and D. Wang, *J. Phys. Chem. C* **113** (2009) 7371.

[30] Y. Huo, J. Zhang, M. Miao and Y. Jin, *Appl. Catal. B* **111–112** (2012) 334.

[31] Y. C. Feng, L. Li, J. W. Li, J. F. Wang and L. Liu, *J. Hazard. Mater.* **192** (2011) 538.

[32] D. Q. Zhang, M. C. Wen, B. Jiang, G. S. Li and J. C. Yu, *J. Hazard. Mater.* **211** (2012) 104.

[33] G. H. Jiang, X. H. Wang, Z. Wei, X. Li, X. G. Xi, R. B. Hu, B. L. Tang, R. J. Wang, S. Wang, T. Wang and W. X. Chen, *J. Mater. Chem.* A **1** (2013) 2406.

[34] H. Gnayem and Y. Sasson, *ACS Catal.* **3** (2013) 186.

[35] Z. Shan, W. Wang, X. Lin, H. Ding and F. Huang, *J. Solid State Chem.* **181** (2008) 1361.

[36] S. Y. Chai, Y. J. Kim, M. H. Jung, A. K. Chakraborty, D. Jung and W. I. Lee, *J.* Catal. **262** (2009) 144.

[37] H. Cheng, B. Huang, Y. Dai, X. Qin and X. Zhang, *Langmuir* **26** (2010) 6618.

[38] T. B. Li, G. Chen, C. Zhou, Z. Y. Shen, R. C. Jin and J. X. Sun, *Dalton Trans.* **40** (2011) 6751.

[39] W. Wang, F. Huang, X. Lin and J. Yang, *Catal. Commun.* **9** (2008) 8.

[40] J. Cao, B. Xu, B. Luo, H. Lin and S. Chen, *Catal. Commun.* **13** (2011) 63.

[41] J. Cao, B. Xu, H. Lin, B. Luo and S. Chen, *Chem. Eng. J.* **185** (2012) 91.

[42] L. Chen, S. F. Yin, S. L. Luo, R. Huang, Q. Zhang, T. Hongand and P. C. Au, *Ind. Eng. Chem. Res.* **51** (2012) 6760.

[43] J. Cao, B. Xu, H. Lin, B. Luo and S. Chen, *Dalton Trans.* **41** (2012) 11482.

[44] H. G. Kim, P. H. Borse, J. S. Jang, E. D. Jeong, O. S. Jung, Y. J. Suh and J. S. Lee, *Chem. Commun.* (2009) 5889.

[45] H. Tada, T. Mitsui, T. Kiyonage, T. Akita and K. Tanaka, *Nat. Mater* **5** (2006) 782.

[46] M. D. Hernandez-Alonso, F. Fresno, S. Suarez and J. M. Coronado, *Energy Environ. Sci.* **2** (2009) 1231.

[47] J. Hu, Y. Zhang, B. Liu, J. Liu, H. Zhou, Y. Xu, Y. Jiang, Z. Yang and Z. Q. Tian, *J. Am. Chem. Soc.* **126** (2004) 9470.

[48] H. Tian, J. Li, M. Ge, Y. Zhao and L. Liu, *Catal. Sci. Technol.* **2** (2012) 2351

[49] A. Hagfeldt and M. Gratzel, *Acc. Chem. Res.* **33** (2000) 269.

[50] J. Zhang, F. J. Shi, J. Lin, D. F. Chen, J. M. Gao, Z. X. Huang, X. X. Ding and C. C. Tang, *Chem. Mater.* **20** (2008) 2937.

[51] Z. H. Li, Z. M. Liu, J. L. Zhang, B. X. Han, J. M. Du, Y. N. Gao and T. Jiang, *J. Phys. Chem. B* **109** (2005) 14445.

[52] K. L. Ding, Z. J. Miao, Z. M. Liu, Z. F. Zhang, B. X. Han, G. M. An, S. D. Miao and Y. Xie, *J. Am. Chem. Soc.* **129** (2007) 6362.

[53] I. Yavari, A. R. Mahjoub, E. Kowsari and M. Movahedi, *J. Nanopart. Res.* **11** (2009) 861.

[54] L. Ge, X. Y. Jing, J. Wang, S. B. Jamil, Q. Liu, D. L. Song, J. Wang, Y. Xie, P. P. Yang and M. L. Zhang, *Cryst. Growth Des.* **10** (2010) 1688.

[55] J. Xia, J. Di, S. Yin, H. Xu, J. Zhang, Y. Xu, L. Xu, H. Li and M. Ji, *RSC Adv.* **4** (2014) 82.

[56] G. A. Tompsett, W. C. Conner and K. S. Yngvesson, *ChemPhysChem.* **7** (2006) 296.

[57] I. Bilecka, I. Djerdj and M. Niederberger, *Chem. Commun.* (2008) 886.

[58] J. C. Yu, X. L. Hu, Q. Li and L. Z. Zhang, *Chem. Commun.* (2005) 2704.

[59] S. H. Kim, S. Y. Lee, G. R. Yi, D. J. Pine and S. M. Yang, *J. Am. Chem. Soc.* **128** (2006) 10897.

[60] L. Zhang, X. F. Cao, X. T. Chen and Z. L. Xue, *J. of Colloid and Interface Sci.* **354** (2011) 630.

[61] L. Kong, Z. Jiang, T. Xiao, L. Lu, M. O. Jonesac and P. P. Edwards *Chem. Commun.* **47** (2011) 5512.

[62] J. Zhang, J. X. Xia, S. Yin, H. M. Li, H. Xu, M. Q. He, L. Y. Huang and Q. Zhang, *Colloids Surf. A* **420** (2013) 89.

[63] L. Q. Ye, J. Y. Liu, C. Q. Gong, L. H. Tian, T. Y. Peng and L. Zan, *ACS Catal.* **2** (2012) 1677.

[64] J. Cao, X. Li, H. L. Lin, B. Y. Xu and S. F. Chen, *Appl. Surf. Sci.* **266** (2013) 294.

[65] L. Kong, Z. Jiang, H. H. Lai, R. J. Nicholls, T. Xiao, M. O. Jones and P. P. Edwards, *J. of Catal.* **293** (2012) 116.

[66] L. F. Lu, L. Kong, Z. Jiang, H. H. C. Lai, T. C. Xiao and P. P. Edwards, *Catal. Lett.* **142** (2012) 771.

[67] J. Fu, Y. L. Tian, B. B. Chang, F. N. Xi and X. P. Dong, *J. Mater. Chem.* **22** (2012) 21159.

[68] Y. Bi, S. Ouyang, J. Cao and J. Ye, Phys. Chem. Chem. Phys. **13** (2011) 10071.

[69] Y. Bi, S. Ouyang, N. Umezawa, J. Cao and J. Ye, *J. Am. Chem. Soc.* **133** (2011) 6490.

[70] Z. M. Yang, G. F. Huang, W. Q. Huang, J. M. Wei, X. G. Yan,Y. Y. Liu, C. Jiao, Z. Wan and A. Pan, *J. Mater. Chem. A* **2** (2014) 1750.

[71] W. Yao, B. Zhang, C. Huang, C. Ma, X. Song and Q. Xu, *J. Mater. Chem.* **22** (2012) 4050.

[72] C. Zhankui, S. Mengmeng, Z. Zhi, M. Liwei, F. Wenjun and J. Huimin, *Catal. Comm.* **42** (2013) 121.

[73] Y. S. Xu and W. D. Zhang, *Dalton Trans.* **42** (2013) 1094.

[74] Y. Song, Y. Lei, H. Xu, C. Wang, J. Yan, H. Zhao, Y. Xu, J. Xia, S. Yina and H. Li, DOI: 10.1039/c4dt03242j.

[75] N. Mohaghegh, M. Tasviri, E. Rahimic and M. R. Gholami, *RSC Adv.* **5** (2015) 12944.

[76] L. L. Zhang, H. C. Zhang, H. Huang, Y. Liu and Z. H. Kang, *New. J. Chem.* **36** (2012) 1541.

[77] J. Zhang, K. Yu, Y. Yu, L. L. Lou, Z. Yang, J. Yang and S. Liu, *J. Mol. Catal. A: Chem.* **391** (2014) 12.

[78] Y. K. Jo, I. Y. Kim, J. M. Lee, S. Nahm, J. W. Choi and S. J. Hwang, DOI: 10.1016/j.matlet.2013.09.091.

[79] W. Liu, M. Wang, C. Xu, S. Chen and X. Fu, *Mater. Res. Bull.* **48** (2013) 106.

[80] X. Yang, H. Cui, Y. Li, J. Qin, R. Zhang and H. Tang, *ACS Catal.* **3** (2013) 363.

[81] G. F. Huang, Z. L. Ma, W. Q. Huang, Y. Tian, C. Jiao, Z. M. Yang, Z. Wan and A. Pan, *J. Nanomater.* 2013 (2013) Article ID: 371356.

[82] J. Cao, B. Luo, H. Lin, B. Xu and S. Chen, *J. Hazard. Mater.* **217-218** (2012) 107.

[83] G. T. Li, K. H. Wong, X. W. Zhang, C. Hu, J. C. Yu, R. C. Y. Chan and P. K. Wong, *Chemosphere* **76** (2009) 1185.

[84] N. Zhang, S. Q. Liu, X. Z. Fu and Y. J. Xu, *J. Phys. Chem. C* **115** (2011) 9136.

[85] APHA, 20th ed, Washington, D. C. USA, 2002.

[86] M. Z. Khan, P. K. Mondal and S. Sabir, *J. Hazard. Mater.* **190** (2011) 222

[87] Y. Wang, Z. Shi , C. Fan , X. Wang, X. Hao and Y. Chi, *J. Solid State Chem.* **199** (2013) 224.

[88] M. Thomas, S. K. Ghosh and K. C. George, *Mater. Lett.* **56** (2002) 386.

[89] M. A. Butler, *J. Appl. Phys.* **48** (1977) 1914.

[90] H. Tang, K. Prasad, R. Sanjines, P. E. Schmid and F. Levy, *J. Appl. Phys.* **75** (1994) 2042.

[91] D. Wang, G. Xue, Y. Zhen, F. Fub and D. Li, *J. Mater. Chem.* **22** (2012), 4751

[92] D. Wang, L. Guo, Y. Zhen, L. Yue, G. Xue and F. Fu, *J. Mater. Chem. A* **2** (2014) 11716.

[93] K. Fujihara, S. Izumi, T. Ohno and M. Matsumura, *J. Photochem. Photobiol. A* **132** (2009) 99.

[94] C. H. Wu, H. W. Chang and J. M. Chern, *J. Hazard. Mater.* **137** (2006) 336.

[95] J. Di, J. Xia, Y. Ge, L. Xu, H. Xu, J. Chen, M. He and H. Li, *Dalton Trans.* **43** (2014) 15429.

[96] C. Xu, H. Wu and F. L. Gu, *J. Hazard. Mater.* **275** (2014) 185.

[97] C. Guo, Y. He, P. Du, X. Zhao, J. Lv, W. Meng, Y. Zhang and J. Xu, *Appl. Surf. Sci.* **320** (2014) 383.

[98] X. X. Wei, H. Cui, S. Guo, L. Zhao and W. Li, *J. Hazard. Mater.* **263** (2013) 650.

[99] Y. Y. Li, J. S. Wang, H. C. Yao, L. Y. Dang and Z. J. Li, *J. Mol. Catal. A: Chem.* **334** (2011) 116.

[100] J. Kim, C. W. Lee and W. Choi, *Environ. Sci. Technol.* **44** (2010) 6849.

[101] A. Kudo and Y. Miseki*, Chem. Soc. Rev.* **38** (2009) 253.

[102] H. Ehrenreich and D. Turnbull, *Solid State Physics: Advances in Research and Applications*, Academic Press 1991. p. 3.

[103] X. Zong, H. Yan, G. Wu, G. Ma, F. Wen, L. Wang and C. Li, *J. Am. Chem. Soc.* **130** (2008) 7176.

[104] D. Wang, T. Kako and J. Ye, *J. Am. Chem. Soc.* **130** (2008) 2724.

[105] Y. Wang, X. Li, Y. Wang and C. Fan, *J. Solid State Chem.* **202** (2013) 51.